



1 **A critical evaluation of decadal solar cycle imprints in the MiKlip**
2 **historical ensemble simulations**

3
4 Tobias C. Spiegl¹, Ulrike Langematz¹, Holger Pohlmann², Jürgen Kröger²

5 ¹Institute of Meteorology, Freie Universität Berlin, Berlin, Germany

6 ²Max Planck Institute for Meteorology, Hamburg, Germany

7

8 *Correspondence to:* T. C. Spiegl (tobias.spiegl@met.fu-berlin.de)

9



10 **Abstract**

11 Studies concerning solar-terrestrial connections over the last decades claim to have found evidence that the quasi-
12 decadal solar cycle can have an influence on the dynamics in the middle atmosphere in the Northern Hemisphere
13 during winter season. It has been argued that feedbacks between the intensity of the UV part of the solar spectrum and
14 low latitude stratospheric ozone may produce anomalies in meridional temperature gradients which have the potential
15 to alter the zonal mean flow in mid to high latitudes. Interactions between the zonal wind and planetary waves can
16 lead to a downward propagation of the anomalies, produced in the middle atmosphere, down to the troposphere.

17 More recently it has been proposed that the projection of possible decadal surface solar signals on the North Atlantic
18 Oscillation might lead to a synchronization of the latter via the 11-year solar cycle. Furthermore, it has been claimed
19 that a realistic representation of the solar cycle in climate models may lead to a significant increase of the decadal
20 prediction skill. These conclusions have been debated controversial since then and a confirmation from other
21 modelling groups is missing.

22 In this paper we aim for an unbiased evaluation of possible solar imprints from the middle atmosphere to the surface
23 and with that from head to toe. Thus, we analyze model output from historical ensemble simulations conducted with
24 the state-of-the-art Earth system model MPI-ESM-HR. The target of these simulations was to isolate the most crucial
25 model physics to foster basic research on decadal climate prediction and to develop an operational ensemble decadal
26 prediction system within the MiKlip framework.

27 Based on correlations and multiple linear regression analysis we show that the MPI-ESM-HR simulates a realistic,
28 statistically significant and robust shortwave heating rate and temperature response at the tropical stratopause, which
29 is known from existing studies. However, the dynamical response to this initial radiative signal in the NH during the
30 boreal winter season is rather weak. In this context we find a slight strengthening of the polar vortex in midwinter
31 season during solar maximum conditions in the ensemble mean, which basically agrees with the so-called “top-down”
32 mechanism. The individual ensemble members, however, show a large spread in the dynamical response with opposite
33 sign in response to the solar cycle.

34 We also analyze the possible surface responses to the 11-year solar cycle and review the proposed synchronization
35 between the solar forcing and the North Atlantic Oscillation. We find that the westerly wind anomalies in the lower
36 troposphere as well as the anomalies in the mean sea level pressure are most likely independent from the seasonal



37 march in the middle atmosphere since they mimic positive and negative phases of the Arctic- and North Atlantic
38 Oscillation rather sporadically than in a systematic way.

39 Finally, by applying lead/lag correlations, our results indicate that the proposed synchronization between the solar
40 cycle and the decadal component of the North Atlantic Oscillation might rather be interpreted as a statistical artefact
41 than a plausible physical connection between the solar forcing and quasi-decadal variations in the troposphere.

42



43 1. Introduction

44 The discipline of decadal climate prediction is rather young and a rapidly growing field in climate science. By using
45 initialized climate model simulations, the gap between weather forecasting and long-term climate model projections
46 covering the complete 21st century or beyond is bridged (e.g. Pohlmann et al., 2013; Meehl et al., 2014). By the aid of
47 decadal climate predictions, policymakers can be equipped with an improved decision-making basis allowing for a
48 better planning of necessary water resources, agriculture, energy and infrastructure measures for the near-term future
49 (Mehta et al., 2011). The aim of the German joint research project “Mittelfristige Klimaprognose” (MiKlip) was to
50 establish a new decadal prediction system allowing for a more precise midterm climate forecasting. To this effect,
51 potential driving factors shaping the decadal climate from both anthropogenic and natural sources have been evaluated
52 critically based on large ensemble simulations with the Max Planck Institute for Meteorology Earth System Model
53 (MPI-ESM).

54 One factor that potentially influences tropospheric weather and climate is the variability in the middle atmosphere via
55 stratosphere-troposphere coupling processes. The internal variability in the middle atmosphere during the dynamically
56 active winter and spring seasons is strongly controlled by the variability of Rossby waves, which propagate upward
57 from the troposphere to the middle atmosphere where they break and interact with the zonal-mean flow. The changes
58 in the zonal-mean flow, again, can alter the propagation conditions for planetary scale waves initiating a self-consistent
59 feedback called wave-mean flow interaction (e.g. Andrews 1985). As a result, strong disruptions, born in the middle
60 atmosphere, such as sudden stratospheric warmings (SSWs), which are characterized by a breakdown of the polar
61 vortex, have the potential to propagate downward into lower atmospheric layers and interfere with the tropospheric
62 weather regime (e.g. Baldwin and Dunkerton, 2001). A prominent example for this are Northern Hemisphere (NH)
63 cold air outbreaks which have the tendency to be more frequent and severe in seasons with a weak stratospheric polar
64 vortex (e.g. Huang et al., 2021).

65 A source of variability that might influence the dynamics in the middle atmosphere on the decadal timescale, via a
66 complex feedback between radiation, chemistry and wave-mean flow interaction is thought to be the 11-year solar
67 cycle. Pioneering work concerning the impact of the solar cycle on middle atmosphere dynamics and possible
68 connections to the troposphere goes back to Kodera and Kuroda (2002). Based on a relatively short period of NCEP
69 reanalysis data (1979 – 1998), the authors observed an increase of the tropical stratopause temperature (TST) (at ~50



70 km) during the time of the solar maximum. In their conceptual explanation, this temperature increase leads to a
71 strengthening of the meridional temperature gradient and an intensification of the polar night jet (PNJ) in the winter
72 stratosphere. The stronger westerlies create a barrier for upward propagating planetary waves, which in turn are
73 deflected poleward and break at lower altitudes. The resulting convergence in the Eliassen-Palm flux (EPF) allows the
74 positive wind anomaly to penetrate downward, where it is dragged towards the pole over the winter season. Kodera
75 (2002) argues that the solar induced wind anomalies may advance into the troposphere, where they create a signal in
76 meteorological variables mimicking a positive phase of the North Atlantic Oscillation (NAO). Matthes et al. (2004,
77 2006) studied the proposed “top-down” mechanism by the aid of idealized simulations with an early middle
78 atmosphere 3-dimensional general circulation model (GCM). They found that during solar maximum conditions the
79 polar vortex seems to be stronger especially in November and December and linked this to a positive Arctic oscillation
80 (AO)-like pattern which they found in lower altitudes and to some extent at the surface. The observed pattern weakens
81 in January and changes sign from February on. In subsequent studies comparable results have been found (e.g., Marsh
82 et al., 2007; Schmidt et al., 2010; Ineson et al., 2011; Chiodo et al., 2012; Langematz et al., 2013), however, showing
83 very individual temporal progressions of the signals from the middle atmosphere to the surface varying from December
84 to February and the proposed influence in the North Atlantic region. These earlier studies are often quoted as
85 convincing proof for a “top-down” influence of the 11-year solar cycle in both the middle atmosphere and the
86 troposphere. Complementary to this, Gray et al. (2013) found that the strongest NAO-like solar-induced signals in the
87 North Atlantic (i.e. a positive phase of the NAO) actually seem to appear with a time lag of three to four years after
88 the solar maximum in the respective seasonal winter mean (DJF). However, the observed lags could not be reproduced
89 in coupled atmosphere-ocean simulations conducted by the same group. In the model, the postulated response to the
90 solar cycle in the North Atlantic appears almost in phase with the solar forcing (maximum response between lag year
91 zero to one) (Gray et al., 2013). This discrepancy between observed and simulated lag in the response in the North
92 Atlantic NAO was confirmed in subsequent studies (e.g. Scaife et al., 2013; Andrews et al., 2015).

93 With respect to possible solar induced impacts on NH surface variability in the winter season, Thiéblemont et al.
94 (2015) went one step further. Analyzing a simulation incorporating 150 model years, they claim that the solar forcing
95 synchronizes the decadal component of the NAO variability spectrum, a phase relation they can not find in an
96 experiment without 11-year solar variability. This result has been debated controversially since its publication. Chiodo
97 et al. (2019) found almost identical spectra of the NAO decadal variability in two simulations of 500 model years each,



98 with and without a 11-year solar cycle forcing. Furthermore, they identified NAO patterns in similar time segments in
99 both experiments (forced and unforced). They suspect, therefore, that the alleged surface solar signals in other studies
100 are most likely a result of the internal variability of the NAO itself rather than solar cycle imprints. On the other hand,
101 Drews et al. (2022) most recently argue that the solar cycle near-surface imprints can only shine through during very
102 active solar periods with large amplitudes of the 11-year solar cycle. They also state that during these periods the
103 surface decadal prediction skill would be significantly enhanced if the solar cycle is a vital part of the prediction
104 system.

105 In this publication, we evaluate possible imprints of the 11-year solar cycle in different domains of the atmosphere
106 from the initial solar radiative signal in the tropical upper stratosphere down to the surface in the NH winter season.
107 We analyze the MiKlip historical ensemble simulations conducted with the state-of-the-art Earth system model MPI-
108 ESM-HR, which is the physical basis for the decadal prediction system, which is operational at the “Deutscher
109 Wetterdienst” (DWD) since 2020. The availability of the large amount of output data from the MiKlip historical model
110 ensemble enables us to address the unresolved questions of the solar surface imprint on a more robust statistical basis
111 than is possible in single model simulations. In our study, we aim to identify the role of the solar imprints for the
112 decadal variability of the NAO in winter.

113 This publication is structured as follows. In Section 2 we describe the MPI-ESM, the setup of the analyzed simulations
114 and the applied methodologies to detect potential solar cycle signals in different atmospheric domains. In Section 3,
115 the initial radiative solar signal in the tropical middle atmosphere is evaluated. Subsequently, we concentrate on the
116 dynamical response to the initial solar signal in the NH winter season. Here we show in Section 4 the ensemble mean
117 response and compare individual ensemble members with opposite solar signatures. In Section 5, we derive solar-
118 induced signals near the surface in our simulations and observations. In Section 6, we check our model results with
119 respect to the proposed synchronization between the solar forcing and the NAO. Finally, we summarize and discuss
120 our results in a broader context (Section 7).

121



122 2. **Data and methods**

123 2.1 Model description and experimental design

124 The historical simulations analyzed in this publication have been conducted with the Max Planck Institute for
125 Meteorology Earth System Model in high resolution configuration (MPI-ESM1.2-HR; hereafter called MPI-ESM-
126 HR) at the Deutsches Klimarechenzentrum (DKRZ). MPI-ESM-HR includes the atmospheric general circulation
127 model ECHAM (European Centre Hamburg) version 6.3 (ECHAM6.3) with a horizontal/vertical resolution of
128 T127L95 (corresponds to a ~100 km * 100 km model grid and 95 levels in the vertical with a model top at 0.01 hPa
129 or ~80 km) (Müller et al., 2018). The high vertical resolution allows for an internally generated quasi-biennial
130 oscillation (QBO) in the tropical stratosphere (Pohlmann et al., 2019). Radiative processes are represented using the
131 rapid radiation transfer model for GCMs (RRTM-G) for both the shortwave and longwave part of the electromagnetic
132 spectrum (Iacono et al., 2008). Other diabatic processes, such as vertical mixing by turbulence and moist convection,
133 large-scale convection, and momentum deposition by orographic and unresolved gravity waves are described in more
134 detail in Stevens et al. (2013). Oceanic processes are accounted for in the coupled Max Planck Institute ocean model
135 (MPIOM) with a TP0.4 (0.4° nominal) resolution (Jungclaus et al., 2013). MPI-ESM-HR further incorporates the
136 biogeochemistry module Hamburg Model of the Ocean Carbon Cycle (HAMOCC) (Ilyina et al., 2013; Paulsen et al.,
137 2017) and the land surface model JSBACH (Reick et al., 2013).

138 In this publication, we analyze 10 members of the MPI-ESM-HR historical simulations performed within the German
139 research project MiKlip. The MiKlip historical ensemble simulations include the observed natural and anthropogenic
140 climate drivers, as described in the CMIP5 protocol (Taylor et al., 2013). The individual ensemble members (1 to 10)
141 have been initialized from different model years of a 1850 preindustrial (PI) control simulation and were integrated
142 over the period 1850 to 2005. Here, we focus on the period 1880 – 1999. Thus, a total of 1,200 model years have been
143 evaluated. Since the model does not include interactive atmospheric chemistry, ozone concentrations have to be
144 prescribed. In the MiKlip historical simulations, the merged CMIP5 ozone dataset was used, which consists of a
145 combination of SAGE I+II satellite and radiosonde data in the period 1979 to 2005. To derive earlier ozone
146 concentrations back to 1850, the zonal mean stratospheric time series is extended backwards based on the regression



147 fits and proxy time series of equivalent effective stratospheric chlorine (EESC) and solar variability (Cionni et al.,
148 2011). The solar variability forcing includes all observed solar cycles and follows Lean (2000).

149

150 2.1 Data analysis

151 *Detrending, correlations, filtering*

152 To detrend the sunspot number (SSN) (Source: WDC-SILSO, Royal Observatory of Belgium, Brussels -
153 <https://www.sidc.be/silso/infosnmtot>) and shortwave heating rate time series, a third-degree polynomial function has
154 been fitted to the data, the respective anomalies are shown in Figure 1. The detrended SSN time series has then been
155 correlated (Pearson r) with the detrended tropical stratopause temperature (defined as the mean value between 25°S
156 – 25°N at 1 hPa (Figure 3)). To reduce the degree of internal variability, a Butterworth bandpass filter with cutoff
157 frequencies of 9 and 13 years has been applied to the detrended PNJ time series (defined as the arithmetic mean of
158 the zonal-mean zonal wind between 35°N – 45°N at 1 hPa) (Figure 3). The same Butterworth bandpass filter has
159 also been applied to the zonal-mean zonal wind time series at 10 hPa (zonal mean over 55°N – 65°N) (Figure 3) and
160 the NAO time series. The NAO time series has been calculated by the aid of an EOF analysis conducted for the
161 MSLP data over the Atlantic sector (20 – 80°N, 90°W – 40°E) in the winter season (DJF averaged and individually
162 for December, January and February). The first principal component is then used to describe the NAO variability.
163 The lead/lag correlations (Figure 8) are then calculated between the filtered NAO and SSN time series.

164 *Multiple linear regression*

165 To detect the solar cycle signals in the middle atmosphere (Figures 2, 4 and 5) and in the mean sea level pressure in
166 both observations and model data (Figures 6 and 7), we use an established multiple linear regression (MLR) technique
167 as described in Bodeker et al. (1998). To derive the individual regression coefficients, we use a set of six predictors in
168 the MLR model:

$$169 \quad X(t) = \text{Off.const} + A * \text{CO2}(t) + B * \text{QBO}(t) + C * \text{QBOorth}(t) + D * \text{SSN}(t) + E * \text{Nino3.4}(t) + F * \text{tau}(t) + R(t)$$

170 with:



171 *Off.const = annual cycle; $CO_2(t)$ = increase in the atmospheric CO_2 concentrations, $QBO(t)$ = phase of the QBO*
172 *defined via the zonal-mean zonal wind in 30 hPa ($5^\circ S - 5^\circ N$); $QBO_{orth}(t)$ = the orthogonal of $QBO(t)$; $SSN(t)$ = SSN*
173 *time series; $Nino3.4(t)$ = Nino3.4 times eries; $\tau(t)$ = optical thickness at 550 nm and $R(t)$ = model residuum*

174 The solar related coefficients have been scaled to 180 SSN, which is a good approximation for a mean solar cycle
175 amplitude. To detect potential time lags in the response to the solar cycle at the surface, the solar time series has been
176 shifted in such a way that the solar forcing lags the model data between one and four years.

177

178 **3. The initial radiative solar signal in MPI-ESM**

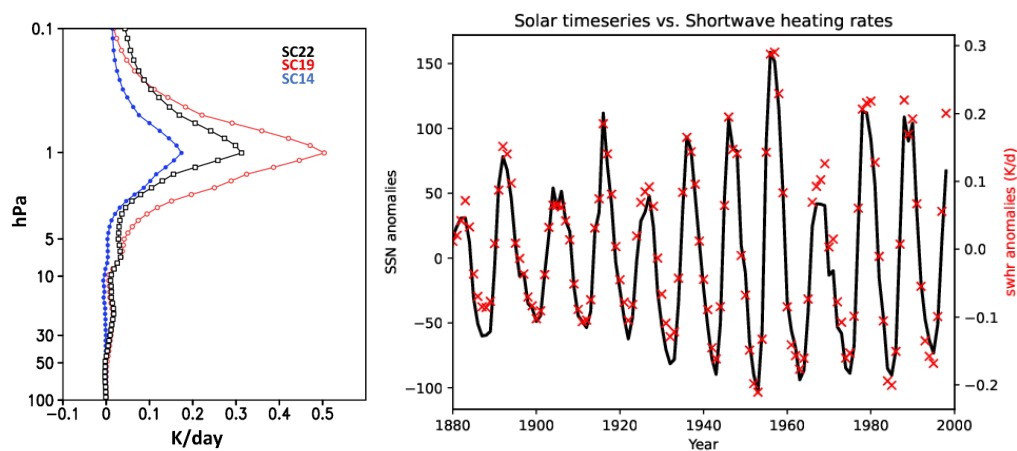
179 The dynamical “top-down” mechanism, assumed to be the pathway for the propagation of the solar signature through
180 the atmosphere to the surface in NH winter (see also Section 1), is initiated at the tropical upper stratosphere by the
181 absorption of solar ultraviolet (UV) irradiance by ozone and molecular oxygen. In particular, the absorption of solar
182 photons by ozone in the Hartley bands (200 – 310 nm) in the upper stratosphere - and to a lesser extent the Huggins-
183 bands (310 nm – 400 nm) in the middle stratosphere – heats the upper stratosphere increasingly with height and leads
184 to the formation of the warm stratopause. Although the variation in solar UV-irradiance over the 11-year solar cycle
185 is less than 10% in the ozone absorption bands, the enhanced UV radiation at solar maximum – in combination with
186 increased ozone concentrations - leads to stronger shortwave heating and a concurrent warming of the tropical
187 stratopause by the order of 1 K, as has been derived from merged MSU4 and SSU+MLS-satellite observations (Randel
188 et al., 2016).

189 Figure 1a shows the annual mean response of the modelled shortwave radiative heating rate (SWHR) at the
190 stratosphere and lower mesosphere (100 – 0.1 hPa) for a range of solar cycle (SC) amplitudes from the weak SC14 (in
191 blue), over the medium SC22 which has been used as solar forcing in the CMIP5 protocol (in green), to the very strong
192 SC19 (in red). MPI-EMS-HR produces the well-known solar cycle impact with enhanced SW heating during solar
193 maximum throughout the upper stratosphere and lower mesosphere. The maximum SWHR difference develops at the
194 stratopause and ranges for the three selected solar cycles between 0.17 and 0.51 K/day. With a SWHR increase of 0.32
195 K/day for the SC22 solar forcing, MPI-ESM-HR produces an initial solar radiative response at the tropical stratopause
196 which is in very good agreement with offline radiation model calculations using the CMIP5 solar forcing (i.e. the same



197 forcing as in MPI-ESM-HR) in a line-by-line reference and two CCM (EMAC and WACCM) radiation codes (see
198 Figure 8, yellow curves in Matthes et al., 2017). This is a significant improvement compared to the earlier ECHAM4
199 and ECHAM5 model versions which were not able to simulate the SWHR response to the solar cycle in the
200 stratosphere (see Figure 17 in Forster et al., 2011), and thus missed the initial solar temperature signal necessary for
201 the “top-down” mechanism. The improvement in the MPI-ESM-HR is the result of the enhanced spectral resolution
202 of the new shortwave radiation scheme in ECHAM6 which resolves the shortwave spectrum in 14 bands spanning the
203 wavelength range from 820 to 50,000 cm^{-1} (Iacono et al., 2008), whereas ECHAM4 and ECHAM5 used a lower
204 spectral resolution with the four-band model of Fouquart and Bonnel (1980), later extended to six bands by Cagnazzo
205 et al. (2007).

206 Figure 1b shows the time series of the SSN and the modeled SWHR at the tropical stratopause over the full simulated
207 period from 1850 – 1999. The shown anomalies of both time series from a third-degree polynomial fit clearly
208 demonstrate that solar cycles of different amplitudes initiate SWHR responses that closely follow in magnitude the
209 strength of the solar forcing. The only exception is found for the weak SC20 which starts from a pretty high minimum.
210 This is not reproduced in the SWHR, possibly due to the transition from synthetic SSN before 1979 to observed SSN
211 afterwards.



212

213 **Figure 1:** Solar shortwave heating rate signature in the MPI-ESM-HR historical simulations: a) Annual tropical
214 mean ($25^{\circ}\text{S} - 25^{\circ}\text{N}$) shortwave heating rate difference in K/day between the maximum and minimum of three solar
215 cycles: the weak solar cycle 14 (blue), the medium solar cycle 22 used in CMIP5 (green), and the strong solar cycle
216 19 (red) (a), and: Time series of the sunspot number and the annual tropical mean ($25^{\circ}\text{S} - 25^{\circ}\text{N}$) shortwave heating
217 rate at the stratopause (1 hPa). Shown are anomalies from a third-degree polynomial fit to the data (b).

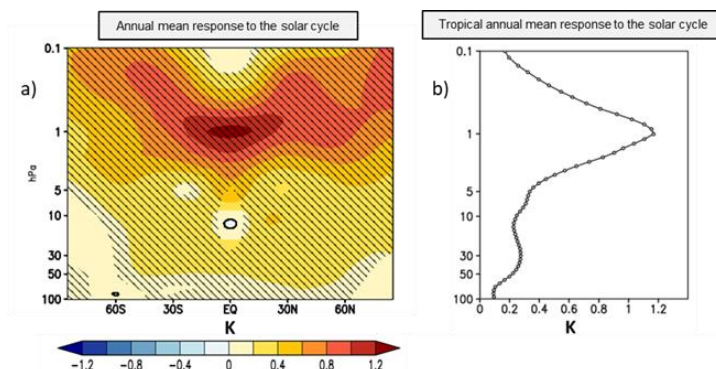


218

219 When averaging over all solar cycles between 1880 and 1999 and all 10 ensemble members, we receive a robust,
220 highly significant annual mean warming of the complete middle atmosphere at solar maximum (Figure 2a), reaching
221 a peak response of 1.2 K at the tropical stratopause (Figure 2b). This result is slightly higher than the solar signal
222 derived from satellite observations (0.7 K/ (100 solar flux units)⁻¹, respectively ~1 K between solar minimum and
223 maximum) (Randel et al., 2016), which is probably due to the relative short time series of satellite observations
224 compared to the simulated time series.

225 Given the excellent temporal evolution of the initial radiative response of the upper tropical stratosphere to the decadal
226 solar forcing, we conclude that MPI-ESM-HR produces the necessary prerequisite for the dynamically enhanced “top-
227 down”-mechanism, which will be investigated in more detail in the next section.

228



229

230

231

232

233

234

235

236

237

238

239

240

241

242

Figure 2: Long-term annual ensemble mean response of the zonal-mean temperature (in K) to the solar cycle in the middle atmosphere as a function of height and latitude (hatched regions mark the 95% level of significance) (a), and the annual mean tropical (25°S – 25°N) temperature response (in K).

4. Downward transfer of the solar signal to the surface: the key role of dynamics

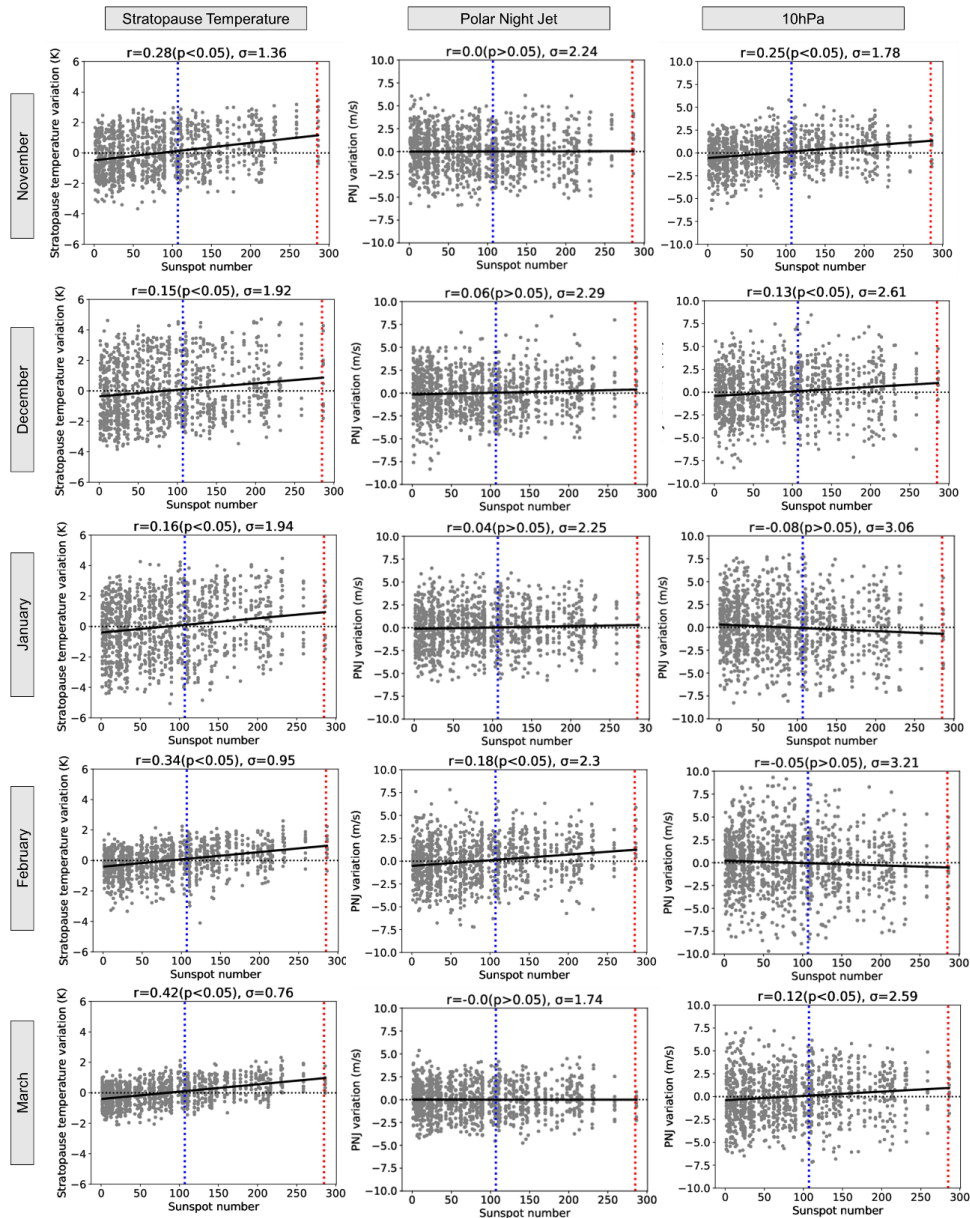
After having demonstrated the ability of the MPI-ESM-HR model to realistically simulate the radiative and the related temperature response in the tropical upper stratosphere to the decadal solar forcing, we investigate as next step the potential dynamical reaction to the radiative forcing, which is expected according to the “top-down” mechanism. By evaluating the ensemble spread in the NH during the dynamically active season (November to March), we assess the



243 variability of different dynamical variables in the stratosphere with respect to the solar fluctuations in the MPI-ESM-
244 HR historical ensemble simulations. We focus first on the detrended deviations from the long-term monthly means for
245 the TST and (to estimate the dynamical response in the NH) the zonal-mean zonal wind at two different altitudes and
246 latitudes (Figure 3). To approximate the PNJ (the local maximum wind speed in the upper stratosphere) we use the
247 mean of the zonal-mean zonal wind in 35°– 45°N at 1 hPa. The variability in the middle stratosphere is represented
248 by the mean of the zonal-mean zonal wind in 55°– 65°N at 10 hPa. After calculating the respective anomaly time
249 series for the TST, the PNJ and the 10 hPa zonal wind variations for each month individually, we correlate these time
250 series with the detrended DJF mean SSN time series. To mute the interannual variability (operating on timescales
251 between 1 and 8 years) of the polar vortex, the PNJ and 10 hPa anomaly time series, as well as the SSN time series,
252 have been bandpass-filtered, before calculating the correlations. Our results indicate that the TST correlates
253 significantly with the SSN, not only in the annual mean (compare Figure 1b) but also in each individual month
254 considered (Figure 3, left column). While negative and positive TST anomalies (i.e. negative and positive deviations
255 from the long-term monthly mean) are almost uniformly distributed for SSN values smaller than the SC14 maximum
256 (blue dotted lines), an increase in the solar forcing exceeding the SC14 SSN maximum leads to a higher probability of
257 positive TST anomalies. The strength of the correlations changes over the season, such that a stronger connection
258 between the solar forcing and the temperature response at the tropical stratopause is given in late autumn (November:
259 $r=0.28$) and late winter (February: $r=0.34$; March: $r=0.42$). In these months, a particular strong solar forcing (indicated
260 by the SSN value of the SC19 maximum (red dotted lines)) is almost always associated with a positive temperature
261 anomaly at the tropical stratopause. Weaker correlations and a broader distribution of negative and positive
262 temperature anomalies, even during periods with especially pronounced solar activity, are calculated for the midwinter
263 season (December: $r=0.15$; January: $r=0.16$). These findings are consistent with an increase in the overall variability
264 in the TST during December and January, making it more difficult for the relatively weak solar induced signals to be
265 distinguished from the background noise. The higher variability in the TST during December and January is probably
266 a result of the higher variability of the tropical branch of the Brewer-Dobson circulation (BDC) in boreal winter.
267 According to the general concept of the “top-down” mechanism the initial signal in the TST would be accompanied
268 by a strengthening of the PNJ via a modification of the meridional temperature gradients. Considering the statistically
269 significant temperature signals and correlations at the tropical stratopause in the MPI-ESM-HR model (Figure 3, left
270 column), we expect a dynamical response of the PNJ in our simulations. However, the correlations between the SSN



271 and the PNJ time series (Figure 3, middle column) do not show statistically meaningful relations between the solar
272 forcing and the dynamical response of the PNJ. Only during February, a weak but statistically significant correlation
273 is found, which might be related to the enhanced impact of the solar forcing in the TST during the same month.
274 However, this connection as well becomes insignificant, if the correlations are calculated based on the unfiltered SSN
275 and PNJ time series. Figure 3 (right column) shows the correlations between the solar forcing and the zonal mean
276 zonal wind for the lower (and more northward) 10 hPa anomaly time series. We find the strongest (and significant)
277 correlations in November ($r=0.25$) and December ($r=0.13$), although these correlations become (again) negligible if
278 the correlations are calculated based on unfiltered model data. The differences in the timing between the maximum
279 correlations of the SSN with the PNJ (February) and the 10 hPa zonal wind time series (November and December) are
280 not in line with the established idea of a successive “poleward and downward” progression of the dynamical solar
281 signal. Furthermore, the computed SSN/PNJ correlations for November, December, January and March are ≤ 0.06 ,
282 implying that the characteristics of the PNJ are not markedly influenced by the magnitude of the solar forcing and thus
283 the amplitude of the solar cycle.



284

285 **Figure 3:** Scatter diagram of the stratopause temperature (left column), PNJ (middle column) and zonal-mean zonal
 286 wind averaged over $55^{\circ}\text{N} - 65^{\circ}\text{N}$ at 10 hPa (right column) variations vs. SSN. The numbers given in the headings
 287 show the correlation coefficients (r), their statistical significance ($p < 0.05$: significant correlation, or $p > 0.05$:
 288 insignificant correlation), and the overall variation (σ). The dotted blue and red lines indicate the SSN at solar cycle
 289 maximum for SC14 and SC19 (the weakest/strongest solar cycles considered in the simulations).

290
 291



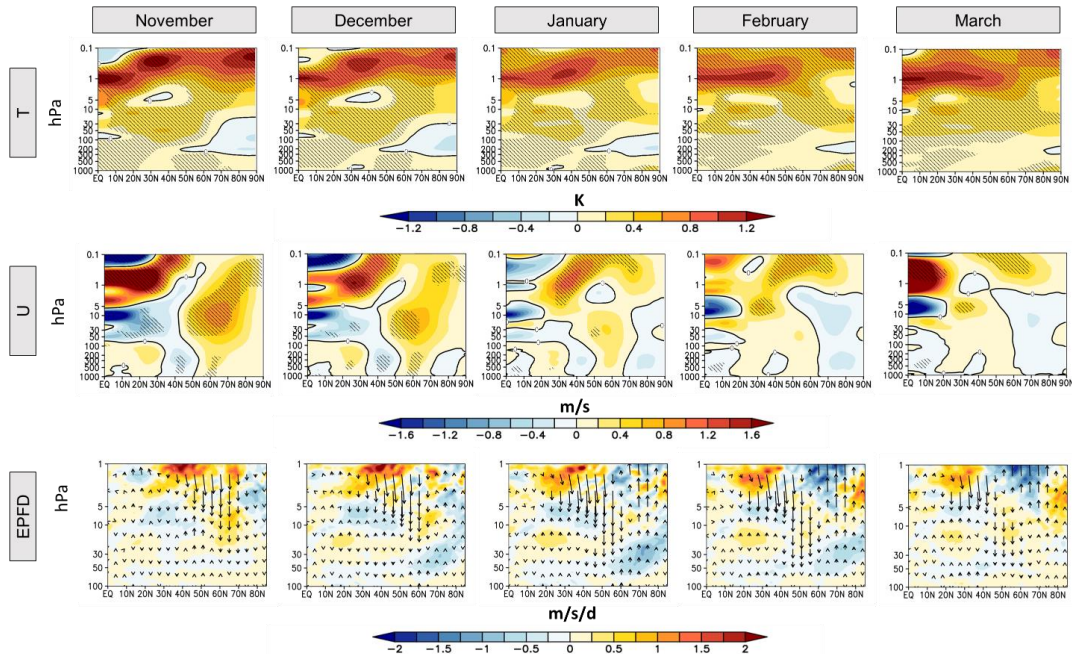
292 Figure 3 demonstrates that while the connection between the solar forcing and the TST is clearly visible in our
293 correlation analysis, the potential dynamical response in the NH is harder to detect, especially due to the highly variable
294 polar vortex. Therefore, we proceed using a MLR analysis to separate the potential dynamical solar induced signals
295 from other internal generated disturbances in the ensemble mean.

296 Figure 4 shows the solar regression coefficients, scaled to a mean amplitude of the solar cycle (180 SSN), for the
297 zonal-mean temperature (top row), the zonal-mean zonal wind (middle row) and the EPF (vectors) and its divergence
298 EPFD (colors) (bottom row) for each NH winter month (November – March). Here, we focus on the potential solar
299 cycle signals between the equator and the North Pole and pressure heights in 1.000 hPa – 0.1 hPa for the temperature
300 and wind responses and 100 hPa – 0.1 hPa for the EPF diagnostics. We find a significant response in the zonal mean
301 temperature at the tropical stratopause (Figure 4, top row) with a maximum response at the equator of 1.2 K during
302 November. The solar induced temperature signal is confined to the inner tropics in late autumn and early winter and
303 advances towards higher latitudes between January and March. This is consistent with the seasonal march of the
304 incidence angle of solar radiation after the winter solstice in December. In the middle to polar latitudes we find a clear
305 dipole in the temperature anomalies especially during November and December. This dipole is characterized by
306 distinct (and significant) positive temperature anomalies in the lower mesosphere and upper stratosphere and weak
307 (and insignificant) negative anomalies in the middle and lower stratosphere. Particularly the pronounced polar heating
308 in the upper stratosphere from November to December agrees well with a most recent analysis of ERA-interim
309 reanalysis data by Kuroda et al., (2022). The detected temperature signals in the middle atmosphere in November and
310 December are in line with the anomalies in the zonal-mean zonal wind (Figure 4, middle row), which indicate a
311 stronger (and thus cooler) polar vortex during these months. Additionally, a convergence of the EPF (indicated by the
312 reddish colors in Figure 4, bottom row) and its (here downward oriented) vectors imply a reduced upward propagation
313 of planetary waves due to the strengthening of the polar vortex. The maximum (and significant) response in the
314 stratospheric zonal-mean zonal wind in the area of the polar vortex, is located at $\sim 60^\circ\text{N}$ at 10 hPa. Here, we find
315 positive anomalies of the zonal-mean zonal wind of ~ 1 m/s. Given the mean zonal-wind speeds between 20 m/s
316 (November) and 30 m/s (December), simulated by the model (not shown) at this height and latitude, the solar influence
317 seems rather small in comparison. The detected dipole in the zonal-mean temperature starts to weaken from January
318 on and vanishes almost completely until March. During the same months, we find a (yet insignificant) weakening of
319 the polar vortex which allows for more upward propagation of planetary waves (indicated by a divergence of the EPF



320 (bluish colors) and upward oriented vectors). In the troposphere, a weak (≤ 0.5 m/s) but significant westerly wind
321 anomaly around $\sim 60^\circ\text{N}$ can be detected in November and December. The weak tropospheric wind response agrees
322 with other studies (Matthes et al., 2006; Schmidt et al., 2010; Ineson et al., 2011; Chiodo et al., 2012; Langematz et
323 al., 2013; Kuroda et al., 2022; Drews et al., 2022).

324 While in some studies the march of the westerly wind anomalies from the middle atmosphere to the surface seems to
325 follow the proposed “poleward and downward” concept (e.g. Matthes et al., 2006; Ineson et al., 2011; Drews et al.,
326 2022), the signal transmission in the MPI-ESM-HR and other model simulations (e.g. Schmidt et al., 2010; Chiodo et
327 al., 2012; Kuroda et al., 2022) rather follows a “downward-only” storyline. Additionally, the description of the
328 westerly wind anomalies at the surface is sometimes inconsistent with the idea of a successive downward propagation
329 of the signal from higher to lower altitudes. As an example, significant westerly wind anomalies at the surface at
330 middle latitudes are already present in November in the modeling studies of Matthes et al. (2006) and Kuroda et al.
331 (2022), even though the major signal is still high up in the middle atmosphere. Furthermore, in Kuroda et al. (2022)
332 the westerly wind anomalies at the surface at middle latitudes are present throughout the complete season (i.e. in all
333 months between November-March), similar to our MPI-ESM-HR simulations. In other studies, the westerly anomalies
334 are insignificant (e.g. Schmidt et al., 2010) or do not reach the ground (e.g. Chiodo et al., 2012). This implies that the
335 detected surface wind anomalies could be independent from the seasonal march in the middle atmosphere and might
336 rather be a product of the internal variability in the troposphere (i.e. the AO or NAO) itself. Likewise, the temperature
337 response to the solar cycle in the troposphere with positive temperature anomalies of ≤ 0.2 K at the surface is rather
338 weak (Figure 4, top row). Interestingly, these small temperature signals are significant in the tropics in all considered
339 months, which is consistent with the high (and relatively constant) solar insolation in the inner tropics and a damped
340 overall variability compared to the extratropical regions. By contrast, the significant surface temperature anomalies in
341 the extratropical regions are located between 50°N and 60°N until January and shift towards the polar latitudes in
342 February and March.



343

344 **Figure 4:** The ensemble mean long-term response to the solar cycle of the zonal-mean temperature (first row), zonal-
345 mean zonal wind (second row) (hatched regions mark the 95% level of significance), and the EPF (vectors) and the
346 divergence of the EPF (EPFD, colors) in the NH during the boreal winter season.

347

348

349 So far, we focussed on the discussion of the potential solar signals in the ensemble mean derived from the 10 individual

350 MiKlip historical simulations thus obtaining statistically more robust results than is possible through analyses of single

351 simulations. The necessity of working with ensemble mean results is impressively demonstrated by comparing two of

352 our 10 individual ensemble members. Figure 5 shows the solar regression coefficients for the zonal-mean temperature

353 and zonal-mean zonal wind for the ensemble members 1 (EM1, top panel) and 4 (EM4, bottom panel), as in Figure 4.

354 The derived patterns for the solar zonal-mean temperature signal in EM1 show distinct similarities with the ensemble

355 mean. As an example, we find a (significant) maximum temperature response around the tropical stratopause.

356 Furthermore, the distribution of the temperature anomalies in the middle to higher latitudes again displays the polar

357 heating in the lower mesosphere and the upper stratosphere and the cooling in the middle to lower stratosphere. Again,

358 this pattern starts to weaken from January on. We notice that in comparison to the ensemble mean, fewer areas depict

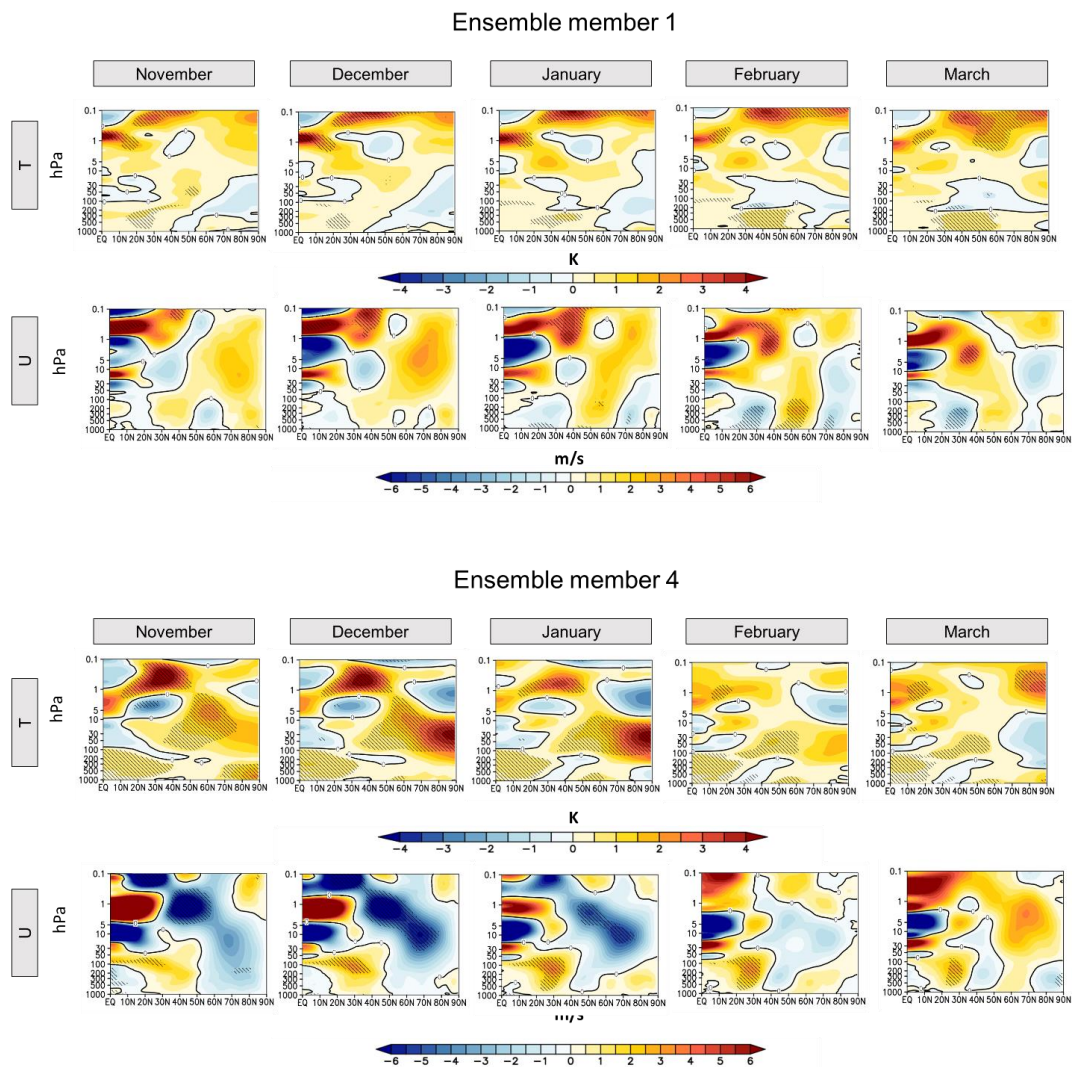
359 significant temperature signals, even though the magnitude of the temperature response is stronger. This can be



360 attributed to the fact that the analysis only includes 120 model years and thus ~12 solar cycles (instead of 1.200 and
361 ~120 in the ensemble mean), which is seemingly not enough to dampen the internal variability and inhibits the solar
362 induced signals to become significant against the overall background noise. Likewise, the solar response of the zonal-
363 mean zonal wind in the middle atmosphere in EM1 shows the main characteristics, as already noticed in the ensemble
364 mean, such as a strengthening of the polar vortex in November and December and a subsequent weakening and a
365 conversion in sign afterwards. However, none of the detected signals in the area of the polar vortex are statistically
366 significant. As for the response of the zonal-mean zonal wind at the surface, we detect significant anomalies in January
367 and February. The geographical distribution of the anomalies (westerly wind anomalies at middle latitudes and easterly
368 wind anomalies at polar latitudes), however, mimic a negative phase of the AO which is not in line with the general
369 concept of solar induced “top-down” influences.

370 In EM4, the initial temperature signal in the upper tropical stratosphere is, as in EM1, visible throughout the complete
371 season and the strongest in November and December. Thus, the response to the solar cycle in these latitudes and
372 heights turns out to be a robust feature in The MPI-ESM-HR model experiments. However, even though exactly the
373 same solar forcing has been applied in EM4 as in EM1, the dynamical response of EM4 looks very different. For
374 instance, we find a cooling of the polar upper stratosphere and a (significant) warming in the middle to lower
375 stratosphere in December and January. This pattern is common during SSWs, which (by chance) could have been
376 more frequent in EM4 during December and January than in EM1. The strong and significant easterly wind anomalies
377 in the middle atmosphere, indicating a slowdown of the polar vortex during these months, underpin this hypothesis.
378 These findings imply that the detected signals in EM1 could also be a result of (by chance) less frequent SSWs in EM1
379 leading to a potentially misleading attribution to solar variability. In our simulations, four out of 10 simulations show
380 a weakening of the polar vortex during high solar activity, while six depict a strengthening of the latter, which may
381 explain the rather weak tendency to westerly wind anomalies in the ensemble mean.

382 Either way, our results point to the fact that the internal dynamics of the polar vortex have the ability to control the
383 transmission of potential solar induced signals from the tropics to the polar regions and are thus more important than
384 the amplitudes of individual solar cycles (compare also Figure 3), as recently claimed by Drews et al., (2022).



385

386 **Figure 5:** Long-term response to the solar cycle of the zonal-mean temperature (first row) and the zonal-mean zonal
387 wind (second row) (hatched regions mark the 95% level of significance) in the two ensemble members EM1 (top
388 panels) and EM4 (bottom panels) in the NH during the boreal winter season.

389

390

391

392

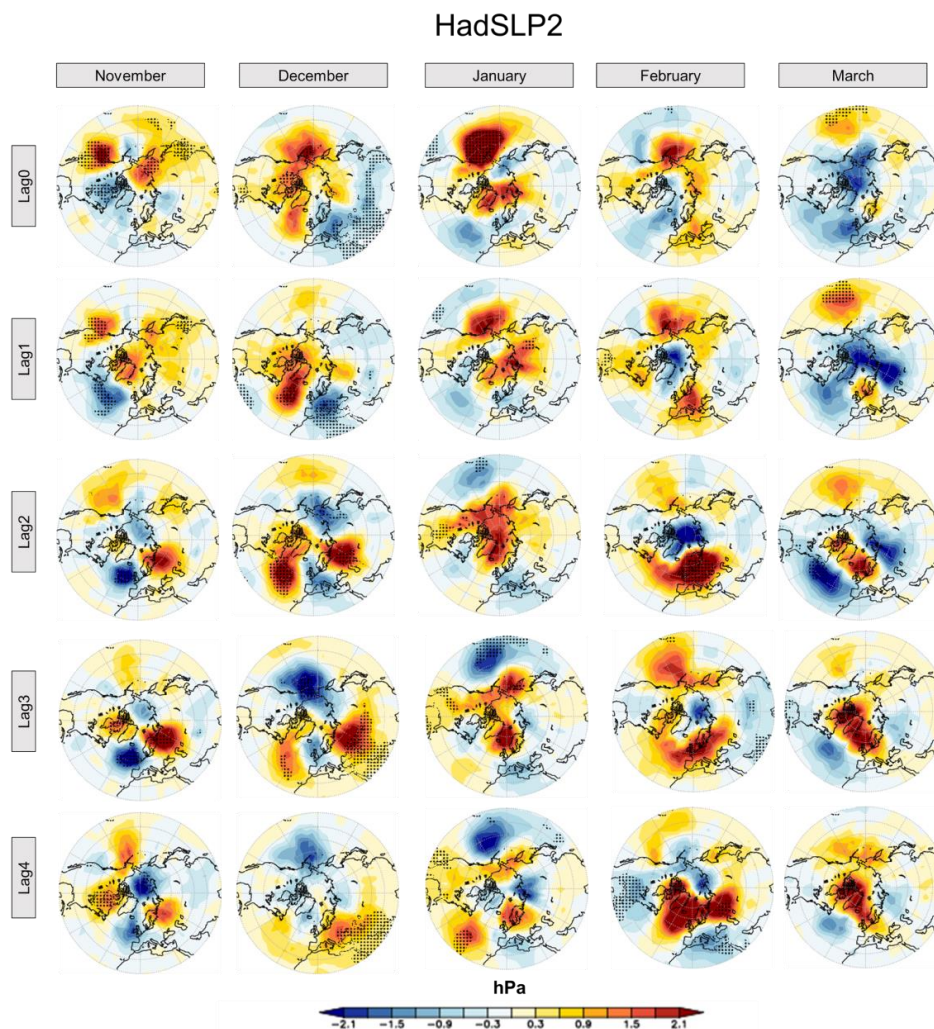


393

394 **5. Direct and lagged surface solar signals**

395 Our results so far indicate a robust response of the TST to the quasi-decadal solar cycle. The subsequent dynamical
396 response in the NH during the boreal winter season, however, is difficult to assess. By the aid of a MLR analysis we
397 could detect weak solar cycle imprints in the zonal-mean temperature and the zonal-mean zonal wind in the ensemble
398 mean. However, these signals are not robust among all individual ensemble members, especially with respect to the
399 detected anomalies in the zonal-mean zonal wind at the surface which seem to be independent of the signals in the
400 middle atmosphere.

401 Nevertheless, in the next step, we first aim at detecting potential solar signals at the surface by applying the MLR
402 analysis to mean sea level pressure (MSLP) data in NH winter. Figure 6 shows the monthly solar regression
403 coefficients for MSLP, scaled to a mean solar cycle amplitude of 180 SSN, in the HadSLP2 observational dataset
404 (Allan and Ansell, 2006) for the same period as simulated (1880 – 1999). In order to check for eventual time lags
405 between the applied solar forcing and the model response, as suggested for example by Gray et al. (2013), lagged
406 regressions were calculated by shifting the solar predictor time series against the observations so that it leads the model
407 data between one and four years. Our results show positive and negative anomalies in the MSLP in the middle and
408 polar latitudes which mimic positive and negative phases of the AO in a rather random than systematic way. As an
409 example, we find an AO-positive like pattern (i.e., negative pressure anomalies over the North Pole and positive
410 pressure anomalies in the surrounding middle latitudes) in November at lag year four, in December at lag year four,
411 in February at the lag years one to three and in March at lag year one. The most pronounced AO-positive anomalies,
412 with a negative but insignificant anomaly of ~2 hPa over the North Pole and a positive anomaly of the same magnitude
413 in the middle latitudes, are given at lag year 2. Hence, the strength of the detected potential solar signals in our
414 HadSLP2 analysis is in line with other studies assessing observational products (e.g., Gray et al., 2013; Kuroda et al.,
415 2022; Drews et al., 2022). The detected maximum impact at lag year 2 in February in our analysis, however, agrees
416 with Kuroda et al. (2022) and Drews et al. (2022) but differs from Gray et al. (2013) who found a maximum response
417 at lag year 4 in the DJF mean. These discrepancies in the timing of the peak solar-induced surface signal in the HadSLP
418 MSLP data can only be explained by differences in the analysis techniques, and reveal a high sensitivity of solar-
419 induced surface signals to the applied methodology and individual interpretation of the results.



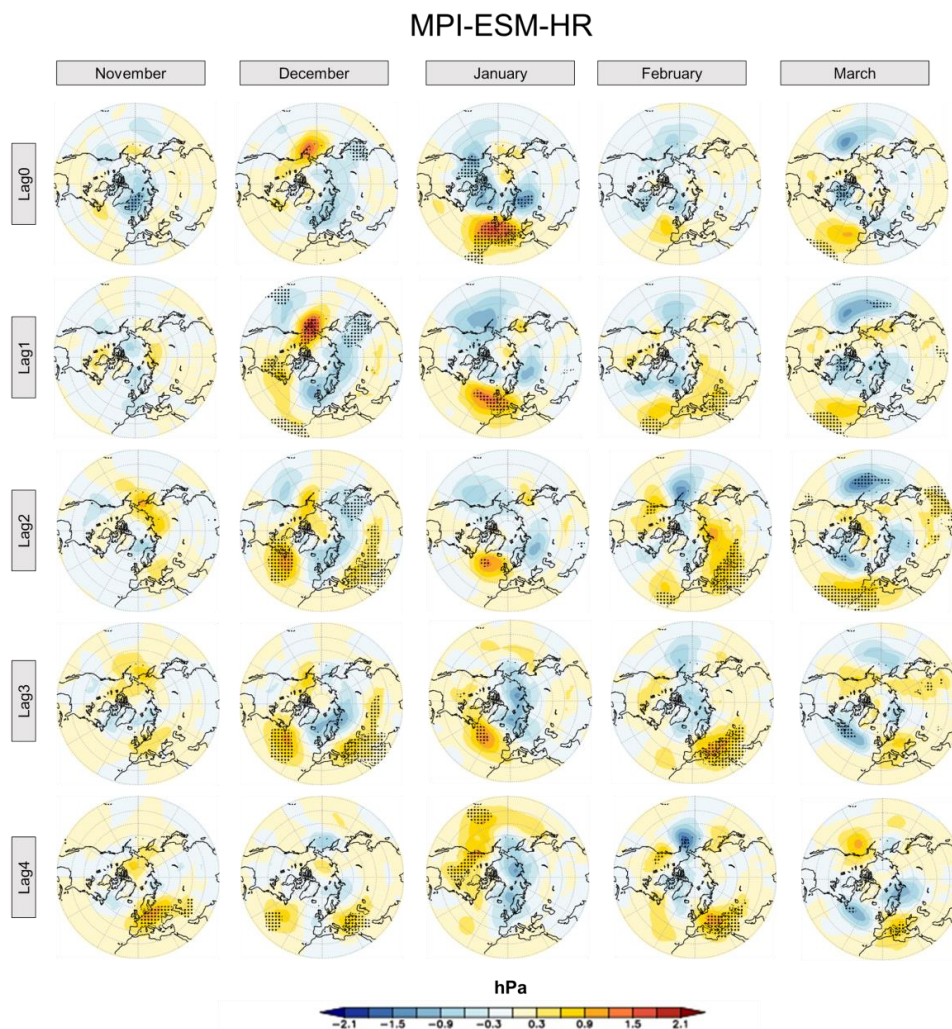
420

421 **Figure 6:** The (lagged) response of mean sea level pressure (MSLP) to the solar cycle in the NH during the boreal
422 winter season for the HadSLP2 dataset (dotted regions mark the 95% level of significance). Columns denote the
423 individual months of the winter season; rows indicate the lag of the MSLP time series with respect to the solar forcing
424 time series.

425



426 Figure 7 shows the same analysis for the MiKlip historical simulations, i.e. the ensemble mean of the solar regression
427 coefficients for the MSLP for each month (November to March) and the (lag) years zero to four. We detect AO-
428 positive-like anomalies in the MSLP in December at the lag years 0 and 1, in January at the lag years 0 to 4 and in
429 February at the lag years zero to four. The strongest negative MSLP anomalies over the North Pole show a response
430 of ~ -1.5 hPa and $\sim +1.5$ hPa in the middle latitudes in January and December. Thus, the overall model response is
431 weaker compared to the observational data. This is not surprising given the fact that the model results depict the mean
432 over 10 ensemble members (with respective dampening effects) compared to one ‘ensemble member’ representing the
433 observations. While the detected magnitudes of the MSLP anomalies in MPI-ESM-HR agree with other solar cycle
434 model studies (e.g. Gray et al., 2013; Scaife et al., 2013; Andrews et al., 2015; Drews et al., 2022), the detected timing
435 (i.e. the progression of the signals from the middle atmosphere to the surface) in the MPI-ESM-HR does not fit the
436 narrative of the “top-down” mechanism as described most recently by Kuroda et al. (2022) and Drews et al. (2022).
437 In these studies, the authors find the most pronounced AO-positive like pattern in February at the surface and link this
438 to the coupling between the stratosphere and the troposphere, which peaks in exactly this month. In contrast, in our
439 model simulations the strongest coupling between the stratosphere and the troposphere appears in December (see
440 Figure 4), while the most pronounced AO-positive like patterns appear in January and February at different lag years.
441 We, therefore, assume that the detected surface solar signals could rather be a product of the internal variability in the
442 troposphere itself than being necessarily a consequence of the proposed “top-down” mechanism. Even if we assume
443 that the detected surface signals have a pure solar source (and the “top-down” mechanism is always present during
444 solar maximum years) it seems to be questionable in our view if these tiny signals would have the capability to
445 synchronize powerful large-scale climate modes such as the AO or the NAO, if they only emerge once per decade
446 over the duration of a month. As an example, the Icelandic Low and the Azores High, both controlling the pressure
447 gradients in the North Atlantic sector, show a month by month variation of ~ 8.5 hPa and ~ 6 hPa during winter time
448 in the model (not shown).



449

450 **Figure 7:** As Figure 6, but for the ensemble mean of the MPI-ESM-HR MiKlip historical simulations.

451

452 **6 A synchronization of the NAO by the solar cycle?**

453 In the following, we will address the question, if the quasi-decadal variations of the solar cycle have the ability to

454 synchronize the decadal component of the NAO, as proposed by Thiéblemont et al., (2015) and Drews et al., (2022).

455 For a better comparison, we apply the same analytical strategy as proposed by Thiéblemont et al. (2015) to our model

456 simulations and the HadSLP2 data, however with the exception that we use the SSN instead of the F10.7 solar flux



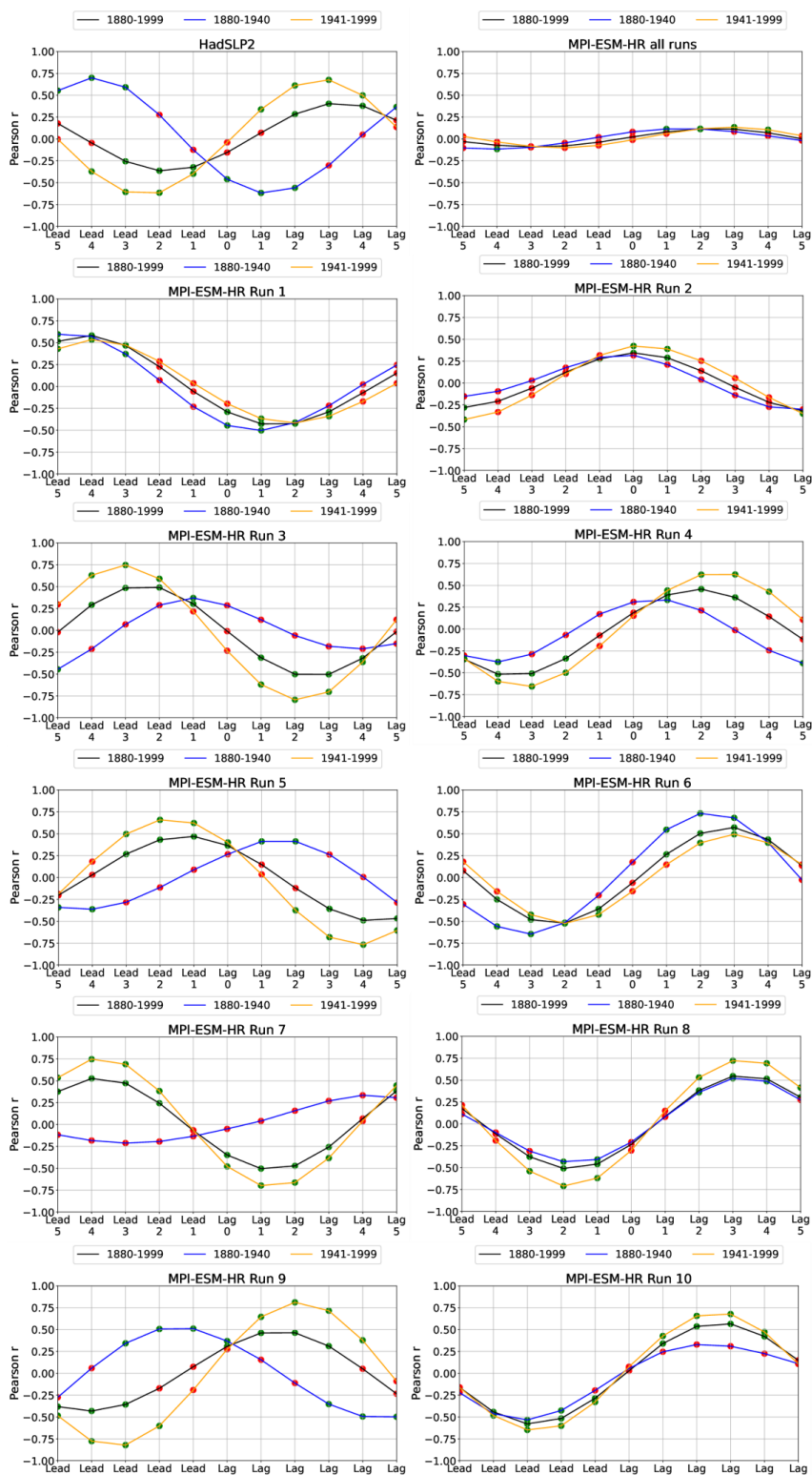
457 times series as a solar proxy. Since both the SSN and F10.7 time series show the same oscillations on the interannual
458 and decadal time scale, this is irrelevant for the interpretation of the results. First, an EOF analysis is applied to the
459 deseasonalized MSLP data over the Atlantic sector (20 – 80°N, 90°W – 40°E) in the winter season (DJF averaged).
460 The resulting leading principal components (PC1) are then used to describe the variability of the NAO. To mute major
461 parts of the interannual variability, we apply a Butterworth bandpass filter with cutoff frequencies of 9 and 13 years
462 to the PC1 and the SSN time series. As a result, the filtered PC1 and SSN time series only include the oscillations
463 operating on the quasi-decadal timescale. Subsequently, lead/lag correlations are calculated between the bandpass-
464 filtered PC1 and SSN timeseries for both the complete dataset and all individual ensemble members (1 to 10). Drews
465 et al. (2022) recently argued that the correlations would become more meaningful during the course of the 20th century
466 due to a series of solar cycles with stronger amplitudes. We, therefore, compute the correlations for three different
467 time segments: the whole period (WP) (1880 – 1999), the early period (EP) with weaker solar amplitudes (1880 –
468 1940) and the late period (LP) with more pronounced solar amplitudes (1941 – 1999).

469 For the HadSLP2 dataset (Figure 8, left column/first row) positive correlations between the decadal variation of the
470 NAO and the solar forcing is found for the lag years one to four in both the WP and the LP periods, with maximum
471 correlations at lag year three during the LP. For the EP, we find an out-of-phase relation between the solar time series
472 and the NAO on the decadal timescale. The evaluation of this (1 ensemble member) observational dataset implies that
473 the solar forcing actually leads the surface response by a couple of years and that this relation is more pronounced
474 during phases of higher solar activity. Indeed, similar phase relations in the different time segments are given in
475 individual ensemble members of the MiKlip historical simulations (e.g. EM9 (Figure 8, left column/sixth row).
476 However, phase relations like these seem far from being a robust feature if all model runs are considered. As an
477 example, EM5 (Figure 8, left column/third row) indicates positive correlations between the decadal behavior of the
478 SSN and the NAO time series for the lag years one to three during the EP, while this relation reverses (showing
479 negative correlations) during the WP and LP. This is also true for EM3 (left column/third row and) and EM7 (left
480 column/fifth row). Other ensemble members (EM2; Figure 8, right column/second row) suggest a maximization of the
481 solar impact at lag year zero and this independently of the considered period. Furthermore, EM6 (Figure 8, right
482 column/fourth row) indicates stronger positive correlations at positive lag years during the EP than during the LP. The
483 most striking discrepancies, however, come from EM1 (Figure 8, left column/second row) and EM4 (Figure 8, right
484 column/third row). While EM1 shows negative correlations between the solar forcing and the NAO at positive lags



485 (in all time segments), this is vice versa in EM4. These surface responses in EM1 and EM4 are, however, opposite to
486 what would be expected from the polar vortex responses in these two ensemble members (a pronounced strengthening
487 of the polar vortex and a downward propagation of westerly wind anomalies to the surface in EM1, and a weakening
488 of the polar vortex and a downward propagation of easterly wind anomalies to the surface in EM4 during winter (see
489 Figure 5)) and opposite to the ‘top-down mechanism’.

490 When applied to the complete dataset of the MiKlip historical simulations, the correlation analysis yields a weak
491 positive (albeit significant) correlation at the lag years two to four, rather independently of the considered time
492 segment. This, however, should rather be interpreted as a slight (and by chance) overhang to positive correlations in
493 the MiKlip dataset (that could change in a larger ensemble) than a robust physical connection between the solar forcing
494 and the NAO. To verify whether the use of the seasonal mean (DJF) might dampen the solar cycle response, as
495 discussed by Drews et al. (2022), we repeated the analysis for the individual winter months (December, January and
496 February, see supplementary material) for the model data. We did not detect stronger connections between the decadal
497 solar forcing and the NAO in the calculations based on individual months compared to the seasonal mean. On the
498 contrary, the correlation analysis based on the December months (i.e., the month where we find the “strongest” “top-
499 down” signals in the middle atmosphere) depicts negative correlations at positive lag years. In summary, given all of
500 these inconsistencies we suspect that there is no robust connection between the quasi-decadal solar oscillations and
501 the respective phase of the NAO in the CMIP5 MiKlip historical ensemble simulations.





503
504
505
506
507

Figure 8: Lead/lag-correlations between the bandpass filtered PC1 based on NAO and SSN time series. For the HadSLP2 dataset and the ensemble mean over the MPI-ESM-HR historical simulations (top row) and the individual MPI-ESM-HR historical runs (rows 2 to 6). Green dots mark statistically significant (95%) correlations.

508

509 7. Summary and discussion

510 Our analysis of the MiKlip historical ensemble simulations, conducted with the state-of-the-art Earth system model
511 MPI-ESM-HR, revealed robust (and statistically significant) solar signals in the TST (see Figures 1 and 2). The
512 dynamical response to the initial solar temperature signal at the tropical stratopause, in the NH middle to polar latitudes
513 during the boreal winter season, however, showed a large spread among our data. This applies to the variability of the
514 PNJ and the 10 hPa zonal-mean zonal wind time series, which both did not show meaningful correlations with the
515 solar forcing (see Figure 3). When removing other than decadal variability components by MLR analysis, we were
516 able to detect (albeit rather weak) solar signals in the NH winter, in both the ensemble mean zonal-mean temperature
517 and zonal-mean zonal wind, that basically agree with the proposed “top-down” influence of solar variability in the
518 middle atmosphere (see Figure 4). However, the MLR analysis based on individual ensemble members revealed
519 signals of opposite direction (i.e. a strengthening (EM1) or weakening (EM4) of the polar vortex during periods of
520 high solar activity) (see Figure 5). Furthermore, we find indications that the detected anomalies in the zonal-mean
521 zonal wind at the surface are most likely independent of the signals in the middle atmosphere. The alleged surface
522 solar signals in MSLP seem to mimic AO-positive (and AO-negative) patterns rather randomly than in a systematic
523 way. This applies to the HadSLP2 data (Figure 6) and to the model data (Figure 7), which both depict most pronounced
524 an AO-positive pattern in January and February at different lag years and thus in months, where the strong stratospheric
525 influence (in December) is already weak or even reverses sign (compare Figure 4). With respect to the suggested
526 synchronization between the decadal solar forcing and the NAO (e.g. Thiéblemont et al., 2015) we can not find any
527 meaningful relations in the MiKlip historical simulations. This is supported by the fact that all ensemble members
528 show very individual phase relations (i.e. positive/negative correlations and maximizations during different lag years)
529 between the solar and the NAO time series. Additionally, more robust correlations could not be achieved in different
530 time segments (i.e. periods with stronger or weaker solar forcing). These findings apply to the seasonal winter mean
531 (DJF) as well as to individual winter months (December, January and February). As a consequence, the detected phase
532 relations in the HadSLP2 dataset should be interpreted carefully with respect to potential physical connections between



533 the solar forcing and the NAO, in particular since the observations represent only one single ensemble member.

534 In summary, we draw four major conclusions:

- 535 1. The decadal variations of the TST in the MiKlip historical simulations are a product of the 11-year solar
536 cycle. In the course of this, an increase in the solar intensity leads to enhanced radiative shortwave heating
537 rates and a warming of the TST. These findings are consistent with other modeling studies concerning the
538 imprints of the 11-year solar cycle in the tropical upper stratosphere (Matthes et al., 2004, 2006; Schmidt et
539 al., 2010; Ineson et al., 2011; Chiodo et al., 2012; Langematz et al., 2013). The solar signals in the TST are
540 statistically significant and robust. They were detected by our correlation and MLR analyses.
- 541 2. The dynamical response of the NH during winter in the middle atmosphere shows a weak strengthening of
542 the polar vortex during solar maximum in the ensemble mean in the MLR analysis. However, the signals
543 (especially in the zonal-mean zonal wind) are mostly insignificant and of opposite sign in individual ensemble
544 members, and thus not a robust feature. We suppose that the dynamical background state in the middle
545 atmosphere (i.e. the variability of the polar vortex) seems to play an important role for the transfer of the
546 initial radiative solar signal from the upper tropical stratosphere down to the troposphere in NH winter.
- 547 3. The detected anomalies in the zonal-mean zonal wind and MSLP at the surface seem not to be related to the
548 seasonal march of the signals in the middle atmosphere and are most likely a manifestation of the internal
549 variability in the troposphere itself.
- 550 4. Concerning the decadal variations of the NAO and the solar forcing, our results suggest that both time series
551 are independent from each other. In this context we find manifold phase relations throughout all of our
552 ensemble members, which implies a statistical by chance relation but not a physical sound connection.

553

554 Since the critical study of Chiodo et al. (2019), the “top-down” mechanism and its surface imprints have been
555 intensively discussed in the scientific community. It is unquestionable that early studies with GCMs and CCMs found
556 evidence of a “top-down” mechanism in the middle atmosphere which in most cases penetrated into the troposphere
557 in NH winter (Matthes et al., 2004, 2006; Schmidt et al., 2010; Ineson et al., 2011; Chiodo et al., 2012; Langematz et
558 al., 2013). These studies all reproduced more or less the basic features of the “top-down” mechanism, thus confirming
559 the physical mechanisms at work, as suggested by Kodera and Kodera (2002). In contrast, more recent simulations
560 with CCMs and ESMs do not seem to find statistical responses of surface variables to the decadal solar forcing (e.g.



561 Chiodo et al., 2019; this study). Only Drews et al. (2022) showed a near-surface solar imprint for solar cycles with
562 strong amplitudes. We suggest that the gradual ‘fading away’ of significant solar near-surface signatures in more up-
563 to-date model studies is closely related to progresses made in model development and computer capacities allowing
564 for ensemble simulations. The early simulations were conducted with fixed lower boundary conditions (i.e. prescribed
565 SSTs from observations or control run experiments) (Matthes et al., 2006; Marsh et al., 2007; Schmidt et al., 2010;
566 Chiodo et al., 2012). Some applied perpetual conditions for the solar forcing (i.e. perpetual solar maximum vs.
567 perpetual solar minimum) and steady-state conditions for the greenhouse gas forcing (Matthes et al., 2006; Marsh et
568 al., 2007; Schmidt et al., 2010; Ineson et al., 2011). In both cases, the complex nature and spectrum of internal
569 variability is damped. Prescribed SSTs, for example, prevent the model from developing the complete spectrum of
570 interannual variability in the troposphere (e.g. induced by the internal variability of the NAO), which might counteract
571 potential surface solar signals. In addition, steady-state background conditions in atmospheric greenhouse gas
572 concentrations and prescribed ozone depleting substances do not take into account transient adjustment processes in
573 the atmospheric dynamics, which again lead to a reduction of the overall internal variability and maybe an
574 overestimation of solar-induced signals. Moreover, due to more limited computer capacities, the results from the early
575 model studies were mostly based on single simulations.

576 In contrast, our results show that in a state-of-the-art climate model system the potential mean solar near-surface
577 signals are rather weak, not robust and inconsistent with the timing in the middle atmosphere. One potential reason is
578 the additional variability component introduced into the model by the interactively coupled ocean model. Misios and
579 Schmidt (2012) also showed the impact of an interactive ocean on the simulated solar response in the tropical Pacific
580 region. While individual ensemble simulations produce the expected phase correlation between the NAO and the solar
581 cycle, others show the opposite behavior. We, thus, do not find any convincing evidence in our model simulations of
582 the alleged decadal synchronization between the NAO and the solar forcing, as suggested by Thiéblemont et al. (2015).
583 In our view, the decadal near-surface signals detected in the MiKlip historical simulations are a product of the internal
584 variability in the troposphere itself and not a physical consequence of the “top-down” mechanism.

585 We would further like to mention that a strong reduction of the interannual variability in two basically independent
586 time series – be it by bandpass filtering like in our study or in Thiéblemont et al. (2015), or by using wide running
587 mean windows like in Drews et al. (2022) – will always lead to significant alignments of these two time series at some
588 point, if they are shifted towards each other gradually. Thus, the phase relations in our (and other studies) seem to be



589 a statistical artifact and not the consequence of a physical phase coupling. We also would like to question if the oceanic
590 memory is sensitive enough to store the tiny surface solar signals (even if there are some) for the duration of a complete
591 decade. Also, please keep in mind the strong variability of the main pressure systems in the North Atlantic, which
592 might wipe out potential surface solar signals within a couple of months. In our opinion, a physically sound explanation
593 for the alleged NAO-solar cycle phase coupling is missing so far. Thus, the claim that an inclusion of the 11-year solar
594 cycle would lead to a better understanding of the decadal oscillations in the NH troposphere during winter, is not
595 supported by our analyses of the MiKlip historical ensemble simulations. Future studies with a distinct focus on the
596 decadal prediction skill might help to confirm our results.

597

598 **Data availability**

599 The main numerical results will be made available upon request by the authors.

600 **Author contributions**

601 TS was in charge in conducting the analysis and writing the manuscript. UL initiated the study and contributed to
602 writing the manuscript. HP and JK were involved in conducting the MiKlip historical simulations and writing the
603 manuscript

604 **Competing interests**

605 The authors do not declare any competing interests.

606 **Acknowledgements**

607 We like to thank the DKRZ for granting the computational resources during MiKlip.

608 **Financial support**

609 BMBF funded projects MiKlip-2 (Förder Kennzeichen 01LP1517A and 01LP1519A) and SOLCHECK
610 (Förder Kennzeichen 01LG1906C)

611 **Review statement**

612 About to come

613



614 **References**

- 615 Allan, R., and Ansell, T.: A new globally complete monthly historical gridded mean sea level pressure dataset
616 (HadSLP2): 1850–2004. *J. Climate*, 19(22), 5816–5842, doi.org/10.1175/JCLI3937.1, 2006.
- 617 Andrews, D. G.: Wave–mean–flow interaction in the middle atmosphere. In *Advances in Geophysics* (Vol. 28, pp.
618 249–275). Elsevier, [doi.org/10.1016/S0065-2687\(08\)60226-5](https://doi.org/10.1016/S0065-2687(08)60226-5), 1985.
- 619 Andrews, M. B., Knight, J. R., and Gray, L. J.: A simulated lagged response of the North Atlantic Oscillation to the
620 solar cycle over the period 1960–2009. *Environmental Research Letters*, 10(5), 054022, [doi:10.1088/1748-](https://doi.org/10.1088/1748-9326/10/5/054022)
621 [9326/10/5/054022](https://doi.org/10.1088/1748-9326/10/5/054022), 2015.
- 622 Baldwin, M. P., and Dunkerton, T. J.: Stratospheric harbingers of anomalous weather regimes. *Science*, 294(5542),
623 581–584. [doi:10.1126/science.1063315](https://doi.org/10.1126/science.1063315), 2001.
- 624 Bodeker, G. E., Boyd, I. S., and Matthews, W. A.: Trends and variability in vertical ozone and temperature profiles
625 measured by ozonesondes at Lauder, New Zealand: 1986–1996. *J. Geophys. Res.*, 103(D22), 28661–28681,
626 doi.org/10.1029/98JD02581, 1998.
- 627 Cagnazzo, C., Manzini, E., Giorgetta, M. A., Forster, P. M. D. F., and Morcrette, J. J.: Impact of an improved
628 shortwave radiation scheme in the MAECHAM5 General Circulation Model, *Atmos. Chem. Phys.*, 7, 2503–
629 2515, <https://doi.org/10.5194/acp-7-2503-2007>, 2007.
- 630 Cionni, I., Eyring, V., Lamarque, J. F., Randel, W. J., Stevenson, D. S., Wu, F., ... and Waugh, D. W.: Ozone
631 database in support of CMIP5 simulations: results and corresponding radiative forcing. *Atmos. Chem. Phys.*,
632 11(21), 11267–11292, doi.org/10.5194/acp-11-11267-2011, 2011.
- 633 Chiodo, G., Calvo, N., Marsh, D. R., and Garcia-Herrera, R.: The 11-year solar cycle signal in transient simulations
634 from the Whole Atmosphere Community Climate Model. *J. Geophys. Res.*, 117(D6),
635 doi.org/10.1029/2011JD016393, 2012.
- 636 Chiodo, G., Oehrlein, J., Polvani, L. M., Fyfe, J. C., and Smith, A. K.: Insignificant influence of the 11-year solar
637 cycle on the North Atlantic Oscillation. *Nature Geoscience*, 12(2), 94–99, doi.org/10.1038/s41561-018-0293-3,
638 2019.



- 639 Drews, A., Huo, W., Matthes, K., Kodera, K., and Kruschke, T.: The Sun's role in decadal climate predictability in
640 the North Atlantic. *Atmos. Chem. Phys.*, 22(12), 7893-7904, doi.org/10.5194/acp-22-7893-2022, 2022.
- 641 Eyring, V., Lamarque, J. F., Hess, P., Arfeuille, F., Bowman, K., Chipperfield, M. P., ... and Young, P. Y.: Overview
642 of IGAC/SPARC Chemistry-Climate Model Initiative (CCMI) community simulations in support of upcoming
643 ozone and climate assessments. *SPARC newsletter*, 40(Januar), 48-66, 2013.
- 644 Forster, P. M., et al.: Evaluation of radiation scheme performance within chemistry climate models, *J. Geophys.*
645 *Res.*, 116, D10302, [doi:10.1029/2010JD015361](https://doi.org/10.1029/2010JD015361), 2011.
- 646 Fouquart, Y., and Bonnel, B.: Computations of solar heating of the earth's atmosphere—A new parameterization,
647 *Beitr. Phy. Atmos.*, 53, 35–62, 1980.
- 648 Gray, L. J., et al.: Solar influences on climate, *Rev. Geophys.*, 48, RG4001, [doi:10.1029/2009RG000282](https://doi.org/10.1029/2009RG000282), 2010.
- 649 Gray, L. J., Scaife, A. A., Mitchell, D. M., Osprey, S., Ineson, S., Hardiman, S., ... and Kodera, K.: A lagged
650 response to the 11 year solar cycle in observed winter Atlantic/European weather patterns. *J. Geophys. Res.*,
651 118(24), 13-405, doi.org/10.1002/2013JD020062, 2013.
- 652 Huang, J., Hitchcock, P., Maycock, A. C., McKenna, C. M., and Tian, W.: Northern hemisphere cold air outbreaks
653 are more likely to be severe during weak polar vortex conditions. *Communications Earth and Environment*,
654 2(1), 147. doi.org/10.1038/s43247-021-00215-6, 2021.
- 655 Iacono, M. J., Delamere, J.S., Mlawer, E.J., Shephard, M. W., Clough, S. A., and Collins, W. D.: Radiative forcing
656 by long-lived greenhouse gases: Calculations with the AER radiative transfer models, *J. Geophys. Res.*, 113,
657 D13103, [doi:10.1029/2008JD009944](https://doi.org/10.1029/2008JD009944), 2008.
- 658 Ilyina, T., Six, K. D., Segschneider, J., Maier-Reimer, E., Li, H., and Núñez-Riboni, I. (2013). Global ocean
659 biogeochemistry model HAMOCC: Model architecture and performance as component of the MPI-Earth system
660 model in different CMIP5 experimental realizations. *J. Adv. Model. Earth Syst.*, 5(2), 287-315.
- 661 Ineson, S., Scaife, A. A., Knight, J. R., Manners, J. C., Dunstone, N. J., Gray, L. J., and Haigh, J. D.: Solar forcing of
662 winter climate variability in the Northern Hemisphere. *Nature Geoscience*, 4(11), 753-757,
663 doi.org/10.1038/ngeo1282, 2011.



- 664 Jungclaus, J. H., Fischer, N., Haak, H., Lohmann, K., Marotzke, J., Matei, D., ... and Von Storch, J. S.:
665 Characteristics of the ocean simulations in the Max Planck Institute Ocean Model (MPIOM) the ocean
666 component of the MPI-Earth system model. *J. Adv. Model. Earth Syst.*, 5(2), 422-446,
667 doi.org/10.1002/jame.20023, 2013.
- 668 Kodera, K.: Solar cycle modulation of the North Atlantic Oscillation: Implication in the spatial structure of the
669 NAO. *Geophys. Res. Lett.*, 29(8), 59-1, doi.org/10.1029/2001GL014557, 2002.
- 670 Kodera, K., and Kuroda, Y.: Dynamical response to the solar cycle. *J. Geophys. Res.*, 107(D24),
671 doi.org/10.1029/2002JD002224, ACL-5. 2002.
- 672 Kuroda, Y., Kodera, K., Yoshida, K., Yukimoto, S., & Gray, L.: Influence of the solar cycle on the North Atlantic
673 Oscillation. *J. Geophys. Res.*, 127(1), e2021JD035519, doi.org/10.1029/2021JD035519, 2022.
- 674 Langematz, U., Kubin A., Brühl, C., Baumgaertner, A.J.G., Cubasch, U., and Spanghel, T.: Solar effects on
675 chemistry and climate including ocean interactions, in *Climate And Weather of the Sun-Earth System*
676 (CAWSES): Highlights from a Priority Program, F.-J. Lübken, ed., Springer, Dordrecht, The Netherlands, 2013.
- 677 Lean, J.: Evolution of the Sun's spectral irradiance since the Maunder Minimum. *Geophys. Res. Lett.*, 27(16), 2425-
678 2428, doi.org/10.1029/2000GL000043, 2000.
- 679 Marotzke, J., Müller, W. A., Vamborg, F. S., Becker, P., Cubasch, U., Feldmann, H., ... and Ziese, M.: MiKlip: a
680 national research project on decadal climate prediction. *Bulletin of the American Meteorological Society*,
681 97(12), 2379-2394, <https://doi.org/10.1175/BAMS-D-15-00184.1>, 2016.
- 682 Marsh, D. R., Garcia, R. R., Kinnison, D. E., Boville, B. A., Sassi, F., Solomon, S. C., and Matthes, K.: Modeling
683 the whole atmosphere response to solar cycle changes in radiative and geomagnetic forcing. *J. Geophys. Res.*,
684 112(D23), doi.org/10.1029/2006JD008306, 2007.
- 685 Matthes, K., Langematz, U., Gray, L. L., Kodera, K., and Labitzke, K.: Improved 11-year solar signal in the Freie
686 Universität Berlin climate middle atmosphere model (FUB-CMAM). *J. Geophys. Res.*, 109(D6),
687 doi.org/10.1029/2003JD004012, 2004.
- 688 Matthes, K., Kuroda, Y., Kodera, K., and Langematz, U.: Transfer of the solar signal from the stratosphere to the
689 troposphere: Northern winter. *J. Geophys. Res.*, 111(D6), doi.org/10.1029/2005JD006283, 2006.



- 690 Matthes, K., Funke, B., Andersson, M. E., Barnard, L., Beer, J., Charbonneau, P., Clilverd, M. A., Dudok de Wit, T.,
691 Haberreiter, M., Hendry, A., Jackman, C. H., Kretzschmar, M., Kruschke, T., Kunze, M., Langematz, U.,
692 Marsh, D. R., Maycock, A. C., Misios, S., Rodger, C. J., Scaife, A. A., Seppälä, A., Shangguan, M., Sinnhuber,
693 M., Tourpali, K., Usoskin, I., van de Kamp, M., Verronen, P. T., and Versick, S.: Solar forcing for CMIP6
694 (v3.2), *Geosci. Model Dev.*, 10, 2247–2302, doi.org/10.5194/gmd-10-2247-2017, 2017.
- 695 Meehl, G. A., Goddard, L., Boer, G., Burgman, R., Branstator, G., Cassou, C., ... and Yeager, S.: Decadal climate
696 prediction: an update from the trenches. *Bulletin of the American Meteorological Society*, 95(2), 243-267,
697 doi.org/10.1175/BAMS-D-12-00241.1, 2014.
- 698 Mehta, V., Meehl, G., Goddard, L., Knight, J., Kumar, A., Latif, M., ... and Stammer, D.: Decadal climate
699 predictability and prediction: where are we?. *Bulletin of the American Meteorological Society*, 92(5), 637-640,
700 doi.org/10.1175/2010BAMS3025.1, 2011.
- 701 Misios, S. and Schmidt, H.: Mechanisms Involved in the Amplification of the 11-yr solar cycle signal in the tropical
702 Pacific Ocean, *J. Climate*, 25, 5102–5118, doi.org/10.1175/JCLI-D-11-00261.1, 2012.
- 703 Müller, W. A., Jungclaus, J. H., Mauritsen, T., Baehr, J., Bittner, M., Budich, R., ... and Marotzke, J.: A higher-
704 resolution version of the max planck institute earth system model (MPI-ESM1. 2-HR). *J. Adv. Model. Earth*
705 *Syst.*, 10(7), 1383-1413, doi.org/10.1029/2017MS001217, 2018.
- 706 Paulsen, H., Ilyina, T., Six, K. D., and Stemmler, I.: Incorporating a prognostic representation of marine nitrogen
707 fixers into the global ocean biogeochemical model HAMOCC. *J. Adv. Model. Earth Syst.*, 9(1), 438-464,
708 doi.org/10.1002/2016MS000737, 2017.
- 709 Pohlmann, H., Müller, W. A., Kulkarni, K., Kameswarrao, M., Matei, D., Vamborg, F. S. E., Kadow, C., Illing, S.,
710 and Marotzke, J.: Improved forecast skill in the tropics in the new MiKlip decadal climate predictions, *Geophys.*
711 *Res. Lett.*, 40, 5798–5802, [doi.10.1002/2013GL058051](https://doi.org/10.1002/2013GL058051), 2013.
- 712 Pohlmann, H., Müller, W. A., Bittner, M., Hettrich, S., Modali, K., Pankatz, K., and Marotzke, J.: Realistic quasi-
713 biennial oscillation variability in historical and decadal hindcast simulations using CMIP6 forcing. *Geophys.*
714 *Res. Lett.*, 46(23), 14118-14125, doi.org/10.1029/2019GL084878, 2019.



- 715 Randel, W. J., Smith, A. K., Wu, F., Zou, C., and Qian, H.: Stratospheric Temperature Trends over 1979–2015
716 Derived from Combined SSU, MLS, and SABER Satellite Observations, *J. Climate*, 29(13), 4843–4859,
717 doi.org/10.1175/JCLI-D-15-0629.1, 2016.
- 718 Reick, C. H., Raddatz, T., Brovkin, V., and Gayler, V.: Representation of natural and anthropogenic land cover
719 change in MPI-ESM. *J. Adv. Model. Earth Syst.*, 5(3), 459–482, doi.org/10.1002/jame.20022, 2013.
- 720 Scaife, A. A., Ineson, S., Knight, J. R., Gray, L., Kodera, K., and Smith, D. M.: A mechanism for lagged North
721 Atlantic climate response to solar variability. *Geophys. Res. Lett.*, 40(2), 434–439, doi.org/10.1002/grl.50099,
722 2013.
- 723 Schmidt, H., Brasseur, G. P., and Giorgetta, M. A.: Solar cycle signal in a general circulation and chemistry model
724 with internally generated quasi-biennial oscillation. *J. Geophys. Res.*, 115(D1), doi.org/10.1029/2009JD012542,
725 2010.
- 726 Stevens, B., et al.: Atmospheric component of the MPI-M Earth System Model: ECHAM6, *J. Adv. Model. Earth*
727 *Syst.*, 5, 146–172, [doi:10.1002/jame.20015](https://doi.org/10.1002/jame.20015), 2013.
- 728 Taylor, K. E., Stouffer, R. J., & Meehl, G. A.: An overview of CMIP5 and the experiment design. *Bulletin of the*
729 *American Meteorological Society*, 93(4), 485–498. doi.org/10.1175/BAMS-D-11-00094.1, 2012.
- 730 Thiéblemont, R., Matthes, K., Omrani, N. E., Kodera, K., and Hansen, F.: Solar forcing synchronizes decadal North
731 Atlantic climate variability. *Nat. Commun.*, 6(1), 8268, [doi:10.1038/ncomms9268](https://doi.org/10.1038/ncomms9268), 2015.
- 732
- 733